JEE Journal of Ecological Engineering

Journal of Ecological Engineering, 2026, 27(6), 273–288
https://doi.org/10.12911/22998993/217550
ISSN 2299–8993, License CC-BY 4.0

Received: 2025.12.15
Accepted: 2026.04.16
Published: 2026.05.01

Sustainable active bio-composite films based on cassava starch reinforced with durian rind nano cellulose and cinnamon essential oil: Optimization and characterization

Nyoman Puspa Asri[1*], Desak Nyoman Surya Suameitria Dewi[2], Joko Sulistyo[1], Yustiah Wulandari Mirzayanti[3], Hans Rachman[1], Jaclyn Regina Anggara[1], Raymond Hamidy[1], Jian-Ming Chern[4]

[1] Food Technology Program, School of Tourism, Universitas Ciputra, CitraLand CBD Boulevard, Jl. Waterpark Boulevard, Made, Kec. Sambikerep, Surabaya, Jawa Timur 60219, Indonesia
[2] School of Medicine, Universitas Ciputra, CitraLand CBD Boulevard, Jl. Waterpark Boulevard, Made, Kec. Sambikerep, Surabaya, Jawa Timur 60219, Indonesia
[3] Department of Chemical Engineering, Institut Teknologi Adhi Tama Surabaya (ITATS), Surabaya 60117, Indonesia
[4] Department of Chemical Engineering and Biotechnology, Tatung University, 40 Chungshan North Road, 3rd Sec. Taipei, 104, Taiwan
* Corresponding author's e-mail: nyomanasri@gmail.com

ABSTRACT

The development of sustainable active bio-composite films based on cassava starch (CS), reinforced with durian rind cellulose nanofibre (CNF) and functionalised with cinnamon essential oil (CEO), was investigated to valorise agricultural waste. The CNF reinforcement was isolated from durian rind using a TEMPO-mediated oxidation method combined with ultrasonication and subsequently incorporated into the starch matrix along with CEO. Response surface methodology (RSM) with a central composite design (CCD) was employed to model and optimise the effects of CNF and CEO concentrations on mechanical properties, water barrier performance, as well as antibacterial activity. The optimisation process identified an optimal formulation containing 5% CNF and 2% CEO. This formulation yielded a maximum tensile strength of 10.45 MPa and a Young's modulus of 188.2 MPa. Furthermore, the simultaneous presence of CNF and CEO effectively enhanced hydrophobicity, reducing the water absorption capacity to 37.5%. The antibacterial modelling revealed broad-spectrum activity, with a more pronounced effect against Gram-positive bacteria. The films exhibited significant inhibition zones against *Staphylococcus aureus* (up to 2.5 cm) and *Escherichia coli* (up to 1.0 cm), as demonstrated by the response surface plots. These findings confirm that the durian rind-derived CNF combined with CEO is a potent reinforcement for sustainable starch-based active food packaging with tunable mechanical and antimicrobial properties

Keywords: cassava starch, cellulose nanofibre, durian rind, cinnamon essential oil, bio-composite film, response surface method.

INTRODUCTION

Synthetic plastics have dominated many human activities, especially in the food packaging industry [1]. Synthetic plastics are produced from non-renewable petroleum, leading to significant environmental problems, including greenhouse gas emissions that contribute to global warming and other ecological concerns [2, 3]. An estimated 8.3 billion tons of plastic have been produced, with 79% of it accumulating in landfills, posing a significant threat to human health and ecological systems [1]. Stakeholders are encouraging the use of biodegradable polymer-based packaging to address this issue and support the sustainable development goals (SDGs), including cellulose nanofibre (CNF)-based packaging, due to its microbial degradability [4].

CNF holds great promise for developing environmentally friendly, sustainable food packaging solutions, as it exhibits high modulus, low thermal expansion, and high barrier properties that help it resist deformation and block oxygen, thereby maintaining food freshness [5]. CNF is also a very economical and lightweight material, making it widely used in various industries [6]. CNF is derived from cellulose-containing materials, including agricultural waste such as durian peel. Durian peel holds great potential due to its high cellulose content of around 31–35% (dry basis) and its abundance (constituting 70% of the total fruit, producing 62,000 tons of durian peel/year) [5], [7]. The matrix material for biocomposite films is a crucial factor in strengthening CNF, typically being a natural biopolymer, such as starch.

Cassava starch (CS), as one of the starch sources, has the potential to serve as an environmentally friendly source of products and a substitute for petroleum-based products, owing to its biodegradability, renewable nature, cost-effectiveness, and abundant availability (national cassava production reaches 18.3 million tons/year). The starch content in CF is higher than that of other tubers, at around 90% [2]. However, its water vapour barrier properties and low functionality have limited the large-scale use of biopolymer-based films. One solution is to reinforce CNF films with functional fillers such as essential oils. Cinnamon essential oil (CEO) can be utilised as a natural food additive due to its ability to protect humans and food from pathogenic microbes and food spoilage [8]. The use of CEO as an antimicrobial in bio-composite films is relatively new, safe, and non-toxic for food applications. Therefore, researchers innovated a sustainable active food bio-composite film (SABF) based on durian peel CNF (DPCNF) and CEO with a Cassava starch (CS) matrix. This study aimed to synthesise an environmentally friendly SABF as an alternative to synthetic plastics. The study examined the effects of the CNF-to-CEO ratio and a CS matrix on mechanical properties, permeability, and antibacterial activity. Additionally, modelling and optimisation were conducted to determine the optimal ratio of the SAFB components using the response surface methodology (RSM).

METHODS

The methods section provides sufficient detail to facilitate replication of the study. Previously published methods were referenced, and this section described only relevant modifications. The experiment diagram is shown in Figure 1.

Material

The materials used in this study were sourced from several suppliers. Musang King durian peel was obtained from a Hokky supermarket. The chemicals supplied by Merck, Germany, included pure analysis-grade sodium hydroxide (NaOH), sodium hypochlorite (NaOCl), hydrochloric acid (HCl), TEMPO, sulfuric acid (H_2SO_4), and glycerol. Additional materials were sourced from a

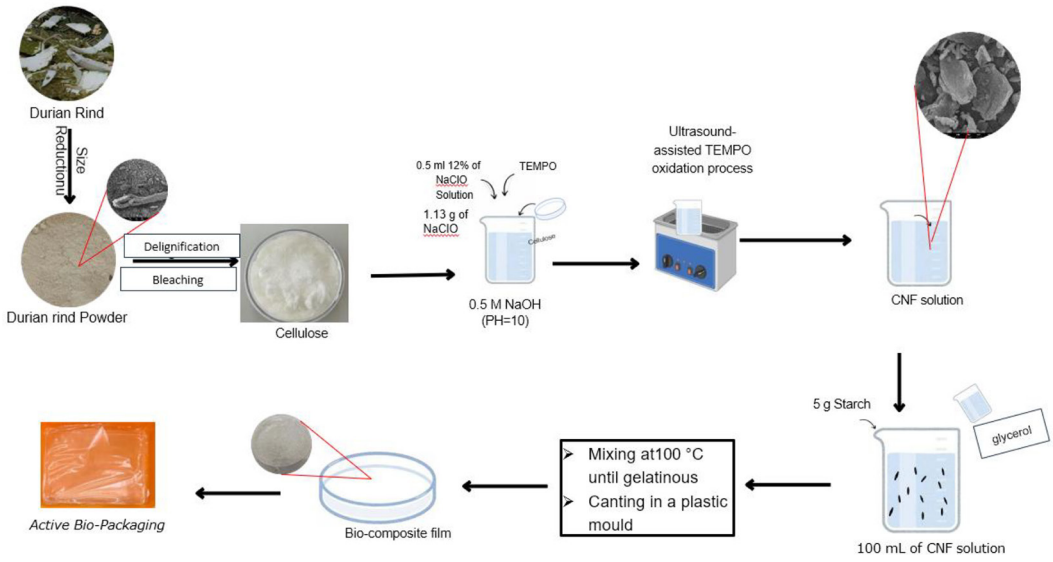

Figure 1. Experiment flow chart

local Indonesian supplier, including cassava flour (Rose Brand, food-grade), cinnamon essential oil, silica gel, nutrient agar, nutrient broth, *Escherichia coli*, and *Staphylococcus aureus*.

Meanwhile, the equipment employed in this study consisted of a grinder, oven, hotplate (VELP Scientifica, Italy), oven (Memmert, Germany), NF-800R centrifuge (Nüve, Turkey), scanning electron microscope (SEM), UV-Vis spectrophotometer SP-UV1100 (Dlab, USA), ATX 224 analytical balance (Shimadzu, Japan), relative humidity (RH) meter (Elitech, China), ultrasonic device, pH meter, disc mill, desiccator, furnace, autoclave, microwave, laminar air flow cabinet, Bunsen burner, and petri dishes.

Durian peel powder preparation

Durian peels obtained from local vendors were first separated from the flesh and then thoroughly washed to remove dirt as well as other impurities. The hard, spiky outer skin of the durian was discarded, while the fibrous inner skin was cut into smaller pieces to facilitate drying. The durian peel pieces were then oven-dried to a low moisture content, resulting in a brittle texture that facilitated easy processing in the next step. After drying, the samples were ground to obtain a more uniform durian peel powder with smaller particles. The ground powder was stored in plastic bags and placed in a desiccator to prevent contamination as well as maintain sample quality. Before delignification, the durian peel powder (DPP) composition was analysed using the Chesson method. Some of the durian peel powder was used for the initial characterisation stage, which included scanning electron microscopy (SEM), x-ray diffraction (XRD), and Fourier transform infrared spectroscopy (FTIR).

Cellulose extraction process from durian peel

Cellulose extraction was performed using the method described by a previous researcher, with slight modifications [8, 9]. The durian peel was dried in an oven at 80 °C for 24 hours, ground using a disc mill, and then sieved. The dried durian peel was then delignified using a 10% NaOH solution at 100 °C for 2 hours under continuous stirring. The obtained solid was washed and neutralised until reaching pH 7. Subsequently, the sample was bleached with a 1.75% NaOCl solution at 75 °C for 30 minutes to remove the colour. The bleached product was then oven-dried until completely dehydrated. After the bleaching process was complete, the sample was oven-dried again until a stable, dry cellulose powder was obtained, ready for analysis or further processing. The extracted cellulose powder was then stored in a sealed container within a desiccator. Storage under these conditions is crucial to prevent moisture absorption from the environment, which could compromise the physical and chemical stability of the cellulose. A portion of this powder was further processed into cellulose nanofibres (CNFs), while another portion was used as the base material for conducting Chesson characterisation. The remaining sample was used for structural analysis through a series of characterisation techniques, namely scanning electron microscopy (SEM), x-ray diffraction (XRD), and Fourier transform infrared spectroscopy (FTIR).

Synthesis of durian peel nanofiber cellulose (DPCNF)

The bleached sample was further converted into nanocellulose according to the method of Hop et al., with modifications [8, 10]. Cellulose was oxidised to nanocellulose using TEMPO, NaBr, 12% NaOCl, and distilled water. The reaction was carried out under ultrasonic treatment, and the solution pH was adjusted to 10 with 0.5 M NaOH. The process was continued until all the NaOH had been completely consumed.

Fabrication of cellulose enriched bio-composite film

A bio-composite film was prepared by solution casting, following the method of Vyas et al., with slight modifications [11]. A total of 5 g of cassava starch, CNF, 12.5% of glycerol, and CEO were dissolved in 100 mL of distilled water and heated at 100 °C under continuous stirring at 1500 rpm until starch gelatinisation occurred. The resulting mixture was then evenly cast into a plastic mould measuring 27 × 19 cm. The mould was dehydrated in an oven at 60 °C for 24 hours before further testing.

Characterisation

Tensile properties were evaluated using a universal testing machine (Zwick/Roell) equipped with TestXpert II software. The testing procedure

was conducted in accordance with ASTM D 882 [12], as described by Patterson et al. [13]. Bioplastic samples with dimensions of 2 × 10 cm were subjected to tensile testing at a pulling speed of 125 mm/min at 25°C. The resulting data were recorded as force values in newtons (N). The tensile strength (*TS*) of the bio-composite films was calculated as the maximum load (F_{max}) divided by the initial cross-sectional area *(A)* of the specimen, as shown in Equation 1. Furthermore, the elongation at break (*EB*) was calculated as the percentage increase in extension at the breaking point (ΔL) over the initial gauge length (L_0), as shown in Equation 2. Finally, Young's modulus (*E*) represents the stiffness of the material and was determined from the slope of the initial linear portion of the stress-strain curve, calculated using Equation 3:

$$TS = \frac{F_{max}}{A} \quad (1)$$

$$EB = \frac{\Delta_L}{L_o} \times 100 \quad (2)$$

$$E = \frac{\sigma}{\varepsilon} \quad (3)$$

where: *TS* is the tensile strength (MPa), F_{max} is the maximum load at break (N), and *A* is the initial cross-sectional area (mm²), *EB* is the elongation at break (%), ΔL is the extension of the specimen at break (mm), and L_O is the initial gauge length (mm), *E* is Young's modulus (MPa), σ is the tensile stress (MPa), and ε is the tensile strain (dimensionless).

The absorbance of the bio-composite film sheets was measured using a UV-vis spectrophotometer at 600 nm against a blank flask [14], as described by Benitez et al. [15]. The transparency of the bioplastic was determined from the transmittance at that wavelength (T600) using Beer-Lambert's law (Equation 4).

$$T_{600} = 10^{2-A} \quad (4)$$

where: T_{600} is the transmittance of the bioplastic (in %) and *A* is the absorbance of the bioplastic at 600 nm (in cm).

The water vapour permeability (WVP) of the bioplastic was determined according to ASTM E-96-00 [16] using the gravimetric method, following the procedure outlined by Mohammad Azmin et al., with modifications [17]. Bioplastic sheets were placed to cover Erlenmeyer flasks containing 2 g silica gel. The flasks were conditioned inside a desiccator (25 °C, 75% relative humidity) using a saturated NaCl solution. WVP was determined from the weight gain of the desiccant after 48 h, according to Equation 5.

$$WVP = \frac{Q}{t} \times \frac{1}{A} \times \frac{L}{P_s(RH_1 - RH_2)} \quad (5)$$

where: *WVP* is the water vapor permeability of the bioplastic (in g m^{-1} day^{-1} Pa^{-1}), Q/t is the mass gain (g day^{-1}), *A* is the surface area of the bioplastic (in m^2), *L* is the thickness of the bioplastic (in m), *Ps* is the saturation pressure at 25 °C (3.17 kPa), RH_1 is the relative humidity in the dessicator (75%), and RH_2 is the relative humidity inside the Erlenmeyer flask (in %).

The antibacterial activity of the bioplastic was tested according to Suryanegara et al. [18] with slight modifications. The antibacterial activity test was performed using Escherichia coli and Staphylococcus aureus, which had been cultured in nutrient broth (NB). A total of 1 mL of bacterial inoculum was transferred into a Petri dish and subsequently mixed with 15 mL of nutrient agar (NA) medium. After the agar solidified, bioplastic samples were cut into 6 mm discs and placed on the agar surface. The plates were then incubated at 37 °C for 24 hours to observe the formation of inhibition zones.

RESULTS AND DISCUSSION

Durian peel characteristics

The chesson data shows significant changes after the durian peel was extracted into cellulose. The soluble portion of the durian peel decreases drastically, as does its hemicellulose content. It differs significantly in its cellulose composition, which increases sharply to 80%. Lignin concentration is reduced by more than half, and the ash content is no longer detected in durian peel cellulose. This change indicates that the extraction process, from delignification to bleaching, is highly effective in separating cellulose from other undesired components (Table 1).

Durian peel commonly contains 35.7% cellulose, 25.3% hemicellulose, and 28.9% lignin;

Table 1. Chesson data

Component	Concentration (%)	
	Durian peel	Durian peel cellulose
Hot water soluble	33.54 ± 0.007	3.49 ± 0.002
Hemicellulose	22.63 ± 0.009	13.9 ± 0.048
Cellulose	35.52 ± 0.009	78.26 ± 0.046
Lignin	8.28 ± 0.002	4.36 ± 0.001
Ash	0.03 ± 0.0001	0 ± 0.000

however, after delignification, the composition changes to 81.4% cellulose, 3.4% hemicellulose, and 3.1% lignin [19]. It could happen because the delignification process can reduce the hemicellulose and lignin content in durian peel. The results of this study are also in line with Putra et al., who stated that the cellulose content after delignification with a strong base solution (alkali method) can reach around 80% [3]. Overall, these data show that durian peel extraction with an alkaline base can reduce non-cellulose components and increase cellulose content. The cellulose structure of durian peel after the delignification and bleaching processes can be described from the SEM image (Figure 2). The SEM results of durian peel cellulose show a more open, hollow structure, and begin to reveal the fibre network. The loss of most of the lignin and hemicellulose weakens the interfibre bonds, making the surface more fibrous and inhomogeneous. This change indicates the success of the process of isolating the cellulose from the lignocellulose matrix. These results are in line with the study by Yong et al., which shows that the isolation of microcrystalline cellulose (MCC) from durian skin produces a more fibrillar and porous structure, which is very different from raw durian skin powder [5]. Another study by Pratiwi et al. stated that the alkali and bleaching processes can open up the cell wall structure so that cellulose fibres are more easily observed on the surface [6].

The FTIR spectra of durian peel cellulose (Figure 3) show several absorption bands that indicate the presence of the main functional groups that make up cellulose. The broad band around 3400 cm^{-1} indicates the stretching of the –OH group associated with intramolecular hydrogen bonds and water still bound to the structure. At around 2900 cm^{-1}, a CH-stretching peak is visible, reflecting the presence of methyl and methylene groups from the cellulose chain. The band in the 1600–1650 cm^{-1} range most likely originates from water molecule bonds (H–O–H), indicating the presence of residual moisture, rather than carbonyl groups. Furthermore, the band at 1300–1400 cm^{-1} represents the C–H or asymmetric vibrations of CH_2 groups in the cellulose network. The sharp band appearing at 1050–1100 cm^{-1} is associated with C–O–C and C–O stretching, indicating the presence of pyranose rings and glycosidic bonds. In addition, the band at around 895 cm^{-1} serves as a diagnostic band characteristic of the β-1,4 glycosidic bonds, which are a major feature of the cellulose structure [5, 7]. The hemicellulose content marked at a band around 1742 cm^{-1} with a C=O group and lignin at a band of 1512 cm^{-1} with a C=C group are still visible in Figure 3 [2].

The XRD analysis (Figure 4) shows the peak of durian peel cellulose at 2θ is around 21 degrees. According to Pratiwi et al., the peak of durian skin cellulose after the bleaching process ranges from 15.76, 22.14, and 34.54 degrees [6]. The peak results obtained are closely related to the crystal domain of the primary cellulose tested. During the delignification and bleaching processes, hemicellulose and lignin components in the amorphous region can be removed so that the crystalline structure dominates the durian peel cellulose sample. Similar to the study by Putro et al., the characteristics of the crystalline phase cellulose of durian peel at 2θ range from 15.1, 16.6, to 23.2 [1]. These results indicate that the

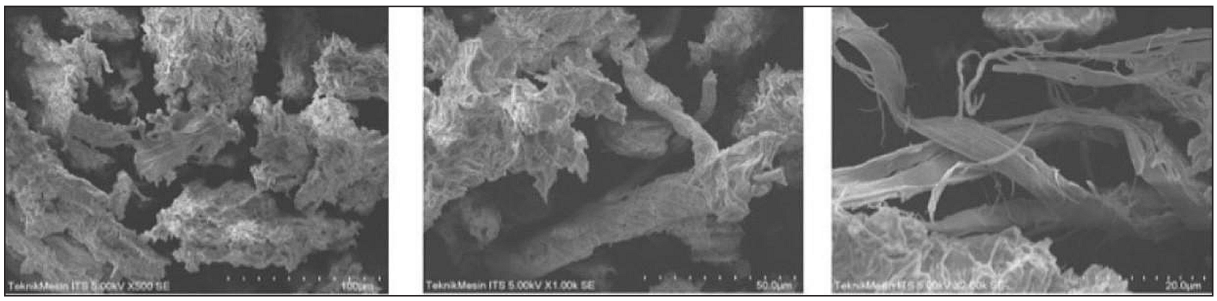

Figure 2. SEM of durian peel cellulose

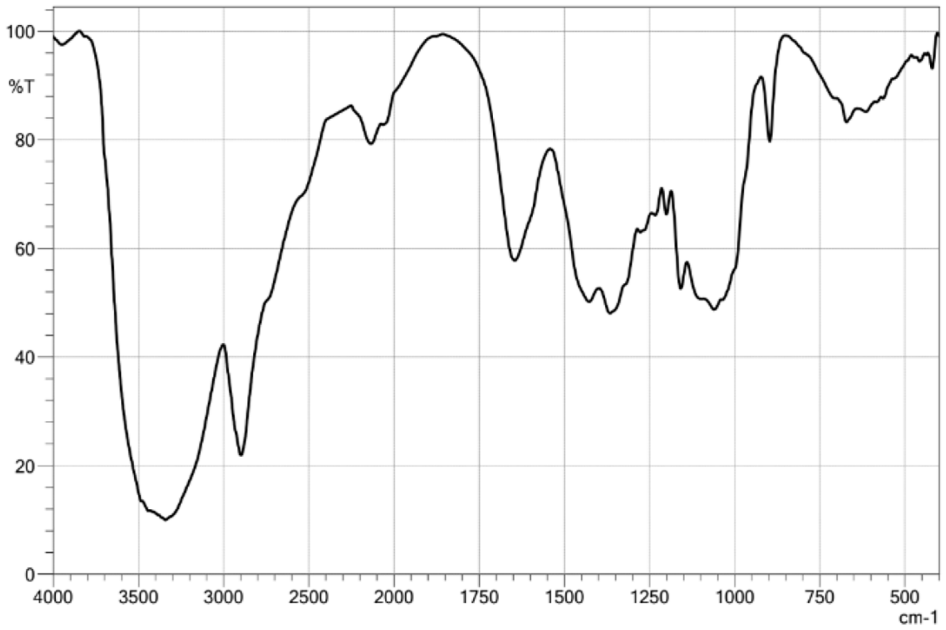

Figure 3. FTIR spectra of durian peel

crystallinity of cellulose is of type 1, which has not changed from the cellulose of durian peel before being separated from other components [19].

Experimental modelling and optimisation

Design Expert version 13 was used to design the experiment. At the same time, response surface methods (RSM) were employed to optimise the process for producing starch biocomposite films, considering two factors: CNF (filler) and CEO (active component) concentration. Each treatment used three levels with codes -1, 0, and +1, corresponding to 1, 3, and 5% and 1, 2, 3% weight relative to the CF matrix, respectively. Meanwhile, the response parameters included tensile strength (TS), per cent elongation (PE), Young's modulus (YM), and water absorbance capacity (WAC). Using the central composite design (CCD), 13 experimental runs were conducted (Table 2).

The experimental results were tested using linear regression to analyse the effect of each treatment. Analysis of variance (ANOVA) was used to analyse the data obtained to determine the interaction between the process and response variables. Accurate and appropriate models were selected at $p < 0.05$ and had a significant correlation. The quality of the proper model was assessed by the coefficients of determination R^2 and adjusted R^2. Then, the two-factor treatment parameters (CNF concentration and CEO concentration) were optimised to construct a desirability index. This optimisation study aimed to reduce WAC while increasing TS, PE, and YM. Therefore, the lowest target response value was for WAC, and the highest for TS, PE, and YM, as indicated by the experimental results obtained.

The process and response variables are connected via polynomial equations derived from RSM. This mathematical modelling, as predicted by RSM, helps explain the relationship between factors and response variables. There are two results of the response surface – the interaction of two factors (2FI) and the quadratic polynomial Equations 6, 7, 8, and 9.

$$TS = 26.35 + 2.44\,A - 2.11\,B + 7.73\,AB \quad (6)$$

$$PE = 2.82 - 0.147\,A - 0.2457\,B - \\ - 0.2912\,A^2 - 0.0663\,B^2 \quad (7)$$

$$YM = 1648.6 + 130.48\,A - 209.93\,B + \\ + 155.25\,AB - 230.36\,A^2 - 151.36\,B^2 \quad (8)$$

$$WAC = 22.36 - 2.63\,A - 3.45\,B + 6.36\,AB \quad (9)$$

The terms A and B (linear), AB (interactive), and A^2 and B^2 (quadratic) represent the model coefficients that describe the interaction between two factors: %CNF (coded by A) and %CEO (coded by B). The synergistic and antagonistic effects of these factors on the response are shown

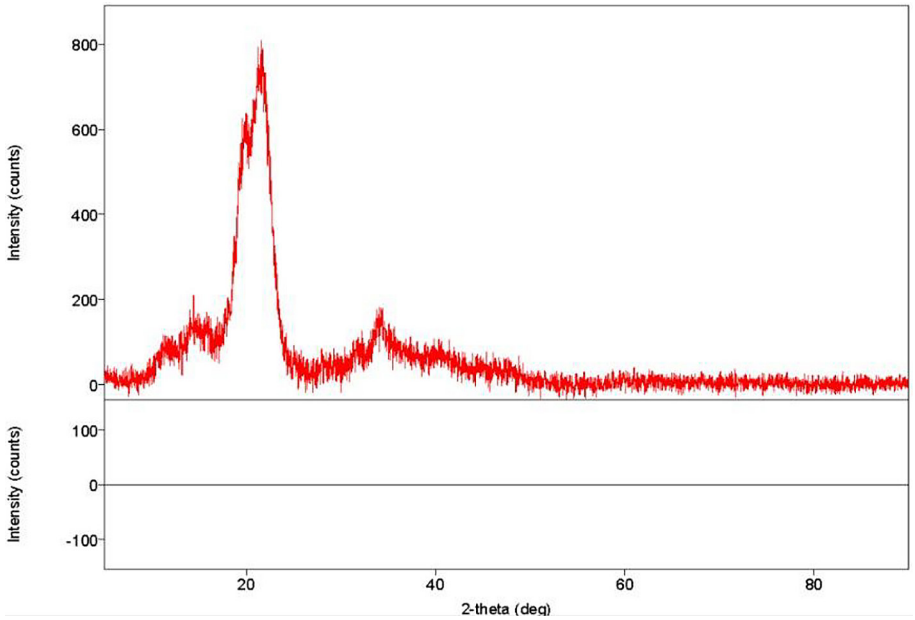

Figure 4. XRD analysis of durian peel

by the positive and negative signs in the equation, respectively [20].

The mechanical performance of the composite films, comprising tensile strength (TS), Young's modulus (YM), and percent elongation (PE), was significantly influenced by the concentration of cellulose nanofibers (CNF) and cinnamon essential oil (CEO).

TS response as a result of the interaction between CNF (1, 3, and 5%) and CEO (1,2 and 3%) can be expressed through a 2FI (two-factor interaction) model, as shown in Table 3. This model was not quite significant at a p-value of 0.2178 due to a low R^2 value of 0.3746, as shown in Table 4. This result describes that the independent parameter does not have a good ability (37.46%) to give the information affecting the tensile strength. The FI model could not be well-aligned with the real data and forecasts because the difference between the adjusted R^2 and predicted R^2 values is more than 0.2.

Table 2. CCD results data

Factor			Response		
(A)	(B)	TS	PE	YM	WAC
CNF (%wt)	CEO (%wt)	(MPa)	(%)	(MPa)	(%)
1	1	32.6	3.1	1300	41.295
5	1	21.8	2.3	1370	20.883
1	3	21	2.4	789	19.774
5	3	41.1	1.6	1480	24.749
0.171573	2	23.6	2.2	1120	20.927
5.82843	2	30.8	2.5	1320	16.999
3	0.585786	33.2	3	1830	22.895
3	3.41421	15.8	2.6	926	15.835
3	2	14.9	3.2	803	20.646
3	2	36.4	2.9	1950	24.209
3	2	18.6	2.8	1620	19.801
3	2	32.5	2.4	2000	20.307
3	2	20.2	2.8	1870	22.44

Table 3. Results of the ANOVA model for the TS response

Source	Sum of squares	df	Mean square	F-value	p-value
Model	321.88	3	107.29	1.8	0.2178
A-CNF	47.45	1	47.45	0.7945	0.396
B-CEO	35.73	1	35.73	0.5983	0.459
AB	238.7	1	238.7	4	0.0766
Residual	537.47	9	59.72	-	-
Lack of fit	186.4	5	37.28	0.4248	0.8135
Pure error	351.07	4	87.77	-	-
Cor. total	859.35	12	-	-	-

Note: *Estimated using a linear regression model developed from the relationship between productive tiller number and observed yield in 2016 and 2018.

Unfortunately, the adequate precision in navigating the design area was not truly signified by the signal at 4.7405, which was the right amount of precision. The coefficient of variance (C.V.%) is a measure of the model repeatability that shows how the standard error compares to the mean of the observed responses. The C.V.% result in this study was 29.33 (C.V.% >10), which means that the model is useful and shows great accuracy as well as consistency based on the experimental values that were collected.

A three-dimensional response surface (Figure 5) shows the graphical regression equations that can be used to identify the optimal interaction conditions. This is a way to describe the state of the interaction system. Figure 4 shows the results of the interaction between factors (CNF and CEO) and responses (TS). In general, TS increases simultaneously with the rise of %CNF and %CEO. As the amount of CNF and CEO in the polymer increases, the tensile strength of the film increases as well. The TS values ranged from 5.5 to 10.5 MPa. The highest TS values (optimal region, indicated in red) were achieved at a high concentration of CNF (5%) combined with a low-to-medium concentration of CEO (1–2%). This improvement in strength is primarily attributed to the reinforcing ability of CNF, which acts as a rigid skeletal framework within the starch matrix, facilitating efficient stress transfer. Adding more CNF will make the hydrogen bonds in the film stronger, which will make the film stronger and more biodegradable. However, an excess of CNF will make biodegradable films weaker. The density and poor particle distribution at high concentrations will make cross-linking in the film less effective, make chains move more freely, and hurt the structure of the polymer matrix [21].

The ANOVA result for elongation shows a quadratic model, as shown in Table 5. This model produces a p-value of 0.2516 with a relatively moderate R^2 value of 0.5489, as shown in Table 6. This result expresses that the independent factor has a moderate ability (54.89%) to explain this effect for PE response. The quadratic model could not be fit with the real data and prediction due to the difference between the adjusted R^2 and predicted R^2 values is more than 0.2. On the other hand, the adequate precision for covering the design area was not truly signified by the value at 3.8606, which was the right amount of precision. The C.V.% result in PE response analysis was 14.74 (C.V.% >10), which means that the model is useful and shows great accuracy and consistency based on the experimental values that were collected.

A three-dimensional response surface (Figure 6) shows the graphical regression equations that can be used to identify the optimal interaction conditions. This is a way to describe the state of the interaction system. Figure 5 shows the results of the interaction between factors (CNF and CEO) and responses (PE). In contrast to the stiffness,

Table 4. Fitting results of the ANOVA model for the TS response

Std. Dev	7.73	R^2	0.3746
Mean	26.35	Adjusted R^2	0.1661
C.V. %	29.33	Predicted R^2	-0.3164
		Adeq. precision	4.7405

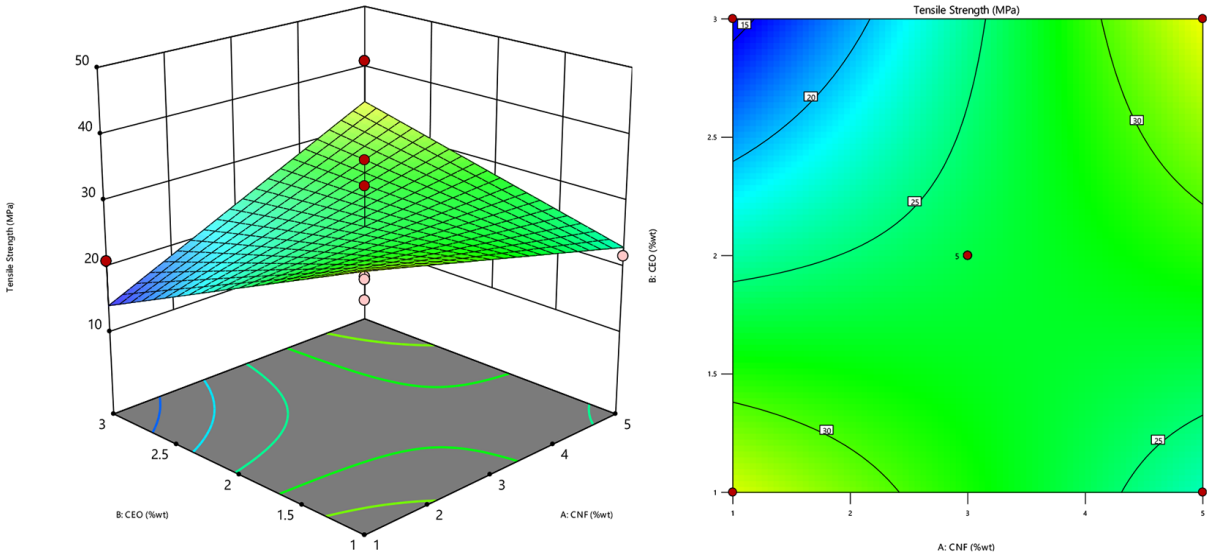

Figure 5. Response surface and contour plot of the TS response

Table 5. Results of the ANOVA model for the PE response

Source	Sum of squares	df	Mean square	F-value	p-value
Model	1.25	5	0.2503	1.70	0.2516
A-CNF	0.1728	1	0.1728	1.18	0.3141
B-CEO	0.4830	1	0.4830	3.29	0.1127
AB	4.441×10^{-16}	1	4.441×10^{-16}	3.023×10^{-15}	1.0000
A^2	0.5901	1	0.5901	4.02	0.0851
B^2	0.0305	1	0.0305	0.2078	0.6623
Residual	1.03	7	0.1469		
Lack of fit	0.7005	3	0.2335	2.85	0.169
Pure error	0.3280	4	0.0820		
Cor. total	2.28	12			

Table 6. Fitting results of the ANOVA model for the PE response

Std. Dev	0.3833	R^2	0.5489
Mean	2.60	Adjusted R^2	0.2267
C.V. %	14.74	Predicted R^2	-1.4095
		Adeq. precision	3.8606

the percent elongation showed a decreasing trend as the CNF concentration increased. While the maximum elongation (peaking at 3.0%) was found in the films with lower CNF content, the high rigidity of the nanofibers naturally reduced the elasticity of the matrix. At the optimal point (5% CNF, 2% CEO), the elongation was recorded in the range of 2.2–2.4%. Although this value is lower than the peak, it is acceptable for packaging applications where structural integrity is prioritized over high elasticity.

The ANOVA result for Young's modulus shows a quadratic model, as shown in Table 7. This model was not quite significant at a p-value of 0.3515 due to a low R^2 value of 0.4876, as shown in Table 8. This result describes that the independent parameter does not have a good ability (48.76%) to give information affecting the Young's modulus. The quadratic model could not be well-aligned with the real data and forecasts, because the difference between the adjusted R^2 and predicted R^2 values is more than 0.2. Unfortunately, the adequate precision in navigating the design area was not truly signified by the signal at 3.2399, which was the right amount of precision. The coefficient of variance is a measure of the model repeatability that shows

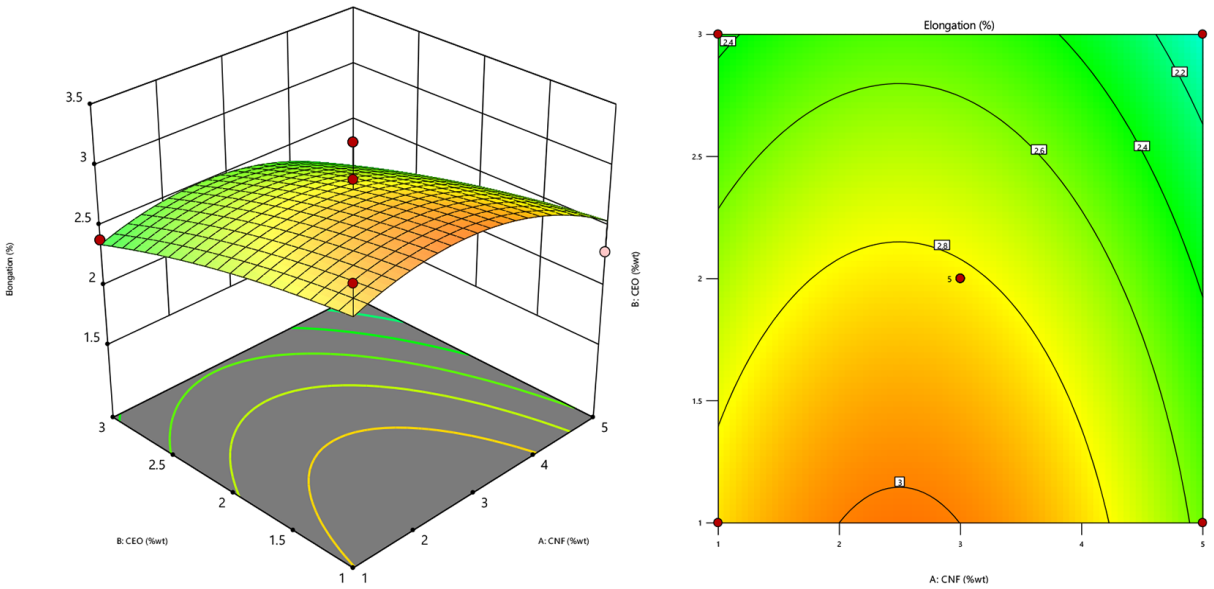

Figure 6. Response surface and contour plot of the PE response

Table 7. Results of the ANOVA model for the Young's modulus response

Source	Sum of squares	df	Mean square	F-value	p-value
Model	1.058×10^6	5	2.117×10^5	1.33	0.3515
A-CNF	1.362×10^5	1	1.362×10^5	0.8572	0.3853
B-CEO	3.526×10^5	1	3.526×10^5	2.22	0.1799
AB	96410.25	1	96410.25	0.6067	0.4615
A^2	3.692×10^5	1	3.692×10^5	2.32	0.1713
B^2	1.594×10^5	1	1.594×10^5	1.00	0.3499
Residual	1.112×10^6	7	1.589×10^5		
Lack of fit	1.331×10^5	3	44358.34	0.1812	0.9040
Pure error	9.792×10^5	4	2.448×10^5		
Cor. total	2.171×10^6	12			

how the standard error compares to the mean of the observed responses. The C.V.% result in this study was 28.20 (C.V.% >10), which means that the model is useful and shows great accuracy as well as consistency based on the experimental values that were collected.

A three-dimensional response surface (Figure 7) shows the graphical regression equations that may be used to find the best interaction circumstances. This is a way to describe the state of the interaction system. Figure 6 shows the results of the interaction between factors (%CNF and %CEO) and responses. Young's modulus consistent with the tensile strength results, exhibited a sharp increase corresponding to the addition of CNF. As it is shown in Figure 6, the modulus values ranged widely from approximately 700 MPa to over 1800 MPa. At the designated optimal composition (5% CNF and 2% CEO), the film exhibited high stiffness with a Young's modulus of approximately 1600–1750 MPa. This substantial increase confirms that the nanofibres successfully restricted the mobility of the starch chains, creating a more rigid network.

The ANOVA result for WAC shows a quadratic model, as it is presented in Table 9. This model was not quite significant at a p-value of 0.0145 due to a low R^2 value of 0.6729, as shown in Table 10. This result describes that the independent parameter does not have a good ability (67.29%) to give information affecting the tensile strength. The FI model could be well-aligned with the real data and forecasts because the difference between the adjusted R^2 and predicted R^2 values is less than 0.2. Unfortunately, the adequate precision in navigating the design area was not truly signified by the signal at 8.6109, which was the right amount of precision. The

Table 8. Fitting results of the ANOVA model for the YM response

Std. Dev	398.62	R^2	0.4876
Mean	1413.69	Adjusted R^2	0.1216
C.V. %	28.20	Predicted R^2	-0.1408
		Adeq. Precision	3.2399

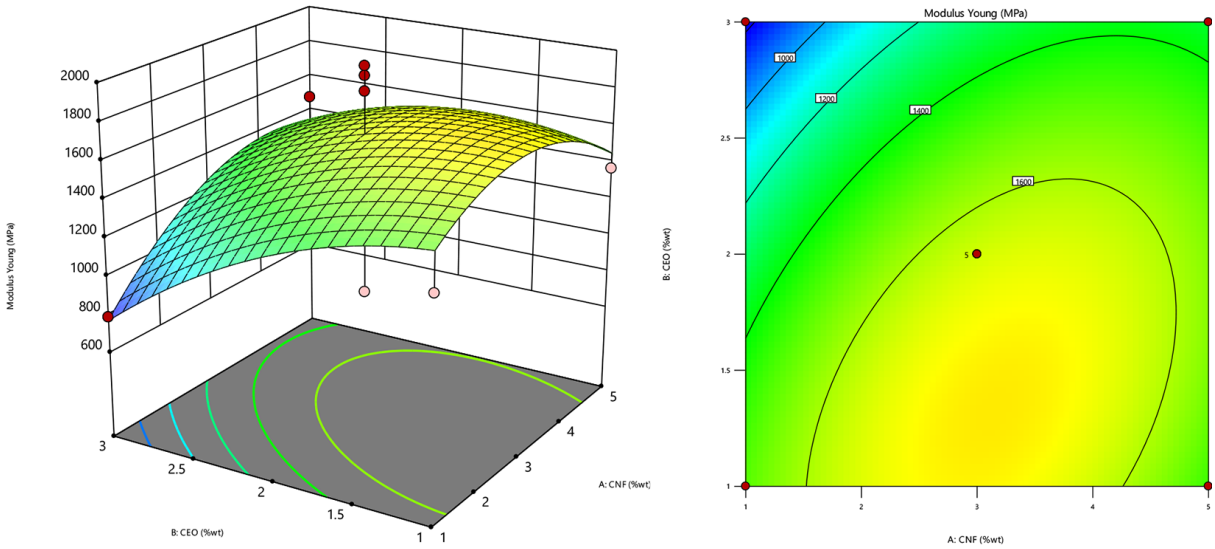

Figure 7. Response surface and contour plot of the Young's modulus response

Table 9. Results of the ANOVA model for the WAC response

Source	Sum of squares	df	Mean square	F-value	p-value
Model	312.25	3	104.08	6.17	0.0145
A-CNF	55.35	1	55.35	3.28	0.1035
B-CEO	95.15	1	95.15	5.64	0.0416
AB	161.76	1	161.76	9.59	0.0128
Residual	151.79	9	16.87		
Lack of fit	138.53	5	27.71	8.36	0.0305
Pure error	13.26	4	3.31		
Cor. total	464.04	12			

coefficient of variance is a measure of the model repeatability that shows how the standard error compares to the mean of the observed responses. The C.V.% result in this study was 18.36 (C.V.% >10), which means that the model is useful and shows great accuracy and consistency based on the experimental values that were collected.

A three-dimensional response surface (Figure 8) shows the graphical regression equations that may be used to find the best interaction circumstances. Water absorption capacity (WAC) is a critical parameter for food packaging applications, where a lower value indicates better water resistance. The experimental results showed that the WAC of the films varied between 35% and 55%. The most desirable properties (lowest WAC, indicated in the blue region of the graph) were obtained in the formulations containing high concentrations of both CNF and CEO.

This phenomenon can be explained by two synergistic mechanisms. First, the CEO possesses strong hydrophobic characteristics, which naturally repel water molecules and reduce the affinity of the film for moisture. Second, the dispersion of CNF effectively fills the pores and void spaces within the tapioca starch matrix. This creates a

Table 10. Fitting results of the ANOVA model for the WAC response

Std. Dev	4.11	R^2	0.6729
Mean	22.36	Adjusted R^2	0.5639
C.V. %	18.36	Predicted R^2	-0.2939
		Adeq. Precision	8.6109

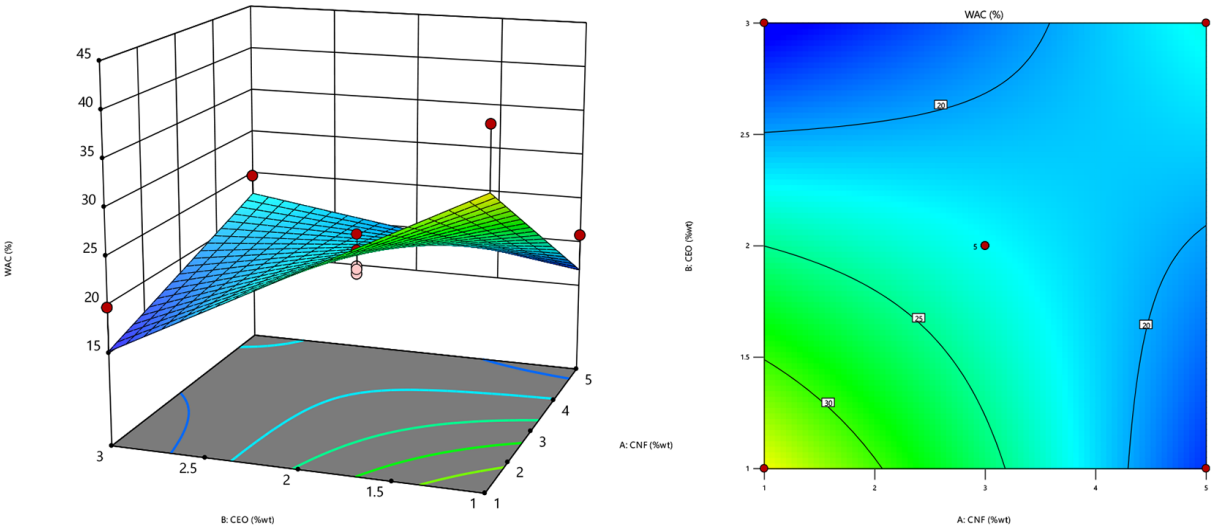

Figure 8. Response surface and contour plot of the WAC response

tortuous path that hinders the diffusion of water molecules, thereby enhancing the barrier performance of the composite films.

Transmitance test

Transmittance (%) is a measure of how much light can pass through a film; higher transmittance generally indicates a more transparent film. In general, transmittance varies widely, ranging from relatively high values (approximately 10–47%) to very low values (0.038–0.1%). The transmittance (T) value appears to decrease drastically as the cinnamon oil concentration increases (for example, from 1.0% CEO with about 10% transmittance to 3.0% CEO with approximately 0.1% transmittance). This trend is reasonable because cinnamon oil is turbid or colored in nature.

The three-dimensional response surface plot (Figure 9) illustrates the relationship between cellulose concentration (Y-axis), cinnamon oil concentration (X-axis), and transmittance (%) (Z-axis).

The response surface shows a sharp decrease in transmittance as the cinnamon oil concentration (X-axis) increases. At low cinnamon oil concentration (1.0%), transmittance reaches its highest level (approximately 45–60%). At high cinnamon oil concentration (3.0%), transmittance decreases drastically to the lowest level (approximately 45%). This confirms that cinnamon oil is the main factor reducing transmittance, making the film more opaque and less transparent.

At low cinnamon oil concentration, increasing the cellulose content (Y-axis) from 1% to 5% appears to slightly increase transmittance (the surface rises from approximately 45% to 60%). At high cinnamon oil concentration, changes in cellulose content have a very small effect because the transmittance is already very low.

Water vapour permeability (WVP)

WVP is a measure of the water vapoir barrier property of a material, and its primary objective is usually to minimise (reduce) the WVP value. This 3D plot maps the log (WVP) values (Z-axis) against cellulose (CNF) and cinnamon oil (CEO) concentrations (Figure 10). Because the Z-axis is presented on a logarithmic scale, lower values on the Z-axis (e.g., −9.7) correspond to better barrier performance (lower WVP). As the cellulose concentration increases (CNF from 1% to 5%), the log(WVP) value tends to increase, as indicated by the upward trend of the response surface

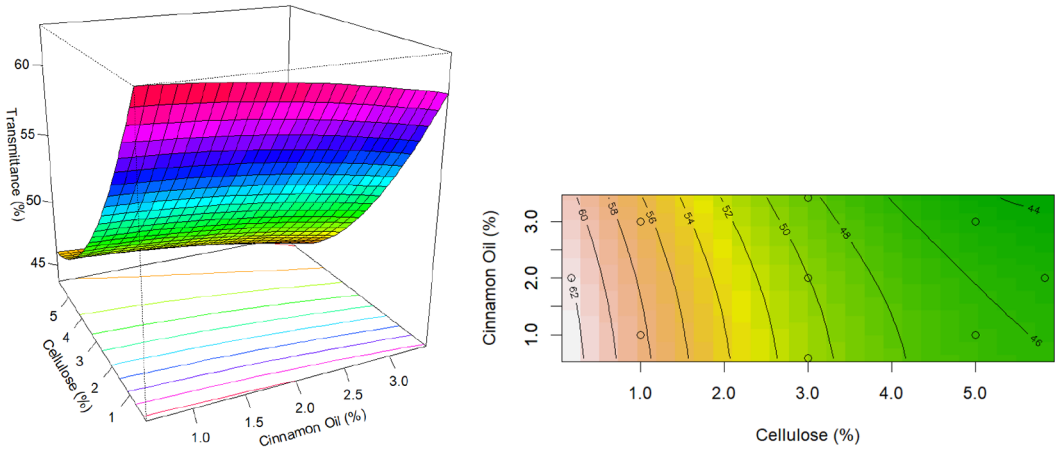

Figure 9. Response surface and contour plot of the transmitance response

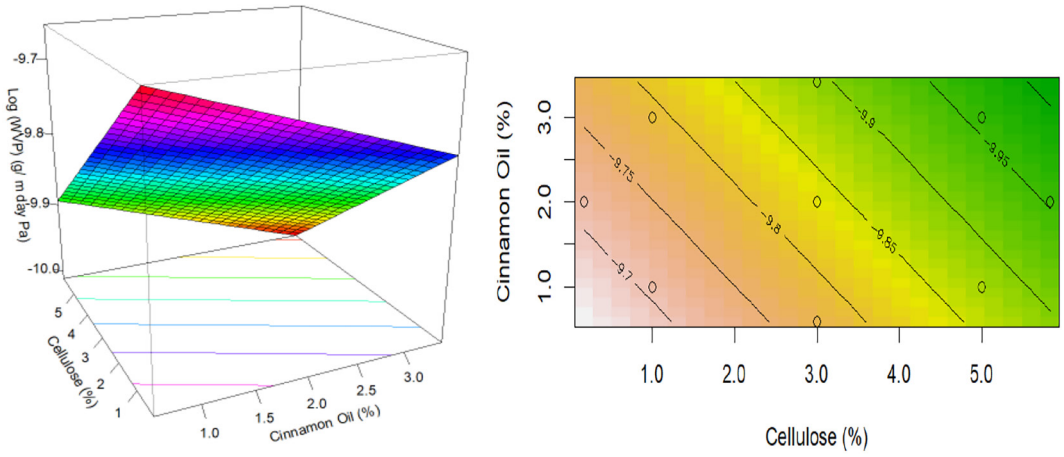

Figure 10. Response surface and contour plot of the WPV response

toward higher log(WVP) values (approaching −9.7). This increase suggests that CNF, due to its hydrophilic nature, increases the WVP of the biocomposite film, thereby reducing its effectiveness as a water vapor barrier.

As the CEO concentration increases (from 1% to 3%), the log(WVP) value tends to slightly decrease, as shown by the downward inclination of the surface toward lower log (WVP) values. This decrease indicates that CEO, as a hydrophobic component, enhances the water vapor barrier properties of the film by reducing WVP. Overall, the response surface appears relatively flat with only a slight slope, suggesting that the interaction between CNF and CEO is not very pronounced compared to the linear effects of each factor.

The contour plot is a two-dimensional projection of the 3D plot, allowing specific factor combinations to be visualised. The values indicated on the contour lines represent log (WVP). The light pink/white area in the lower-left region of the plot exhibits the lowest log(WVP) values (approximately −9.7). The concentration of cellulose (CNF ≈ 1%) and cinnamon oil was low (CEO ≈ 1%). The dark green area in the upper-right region of the plot shows the highest log(WVP) values (approximately −9.95). The cellulose has a high concentration (CNF ≈ 5%), and the concentration of cinnamon oil is also high (CEO ≈ 3%). An anomaly is observed in the contour plot that would not typically be expected in a model optimised for minimisation. The lowest log(WVP) value (−9.7) appears in the lower-left corner (low CNF, low CEO), while the highest log(WVP) value (−9.95) appears in the upper-right corner (high CNF, high CEO). Mathematically, log(WVP) = −9.7 corresponds to WVP = $10^{-9.7}$, whereas log(WVP) = −9.95 corresponds to WVP = $10^{-9.95}$. Since $10^{-9.7} > 10^{-9.95}$, the highest WVP occurs in the light pink/white region (low CNF, low CEO), while the lowest WVP occurs in the dark green region (high CNF, high CEO).

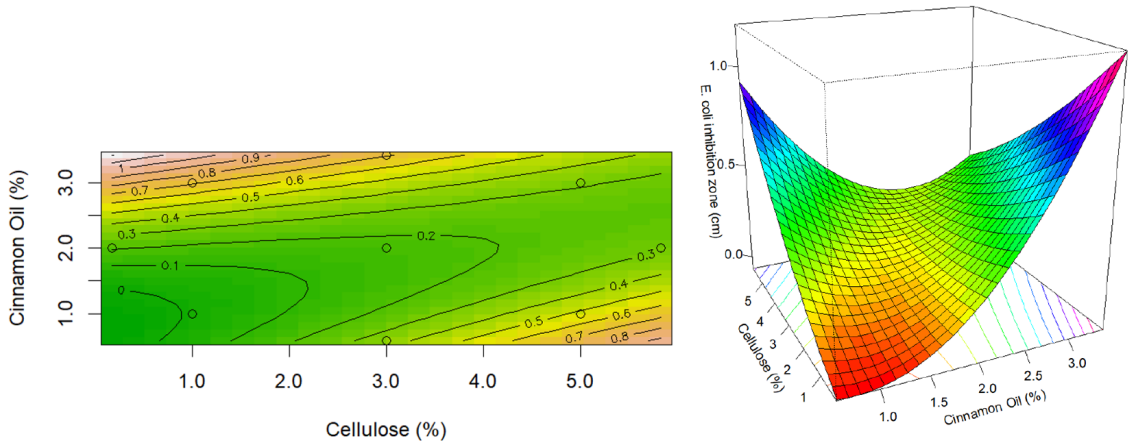

Figure 11. Inhibition zone against *E. coli*: response surface and contour plot

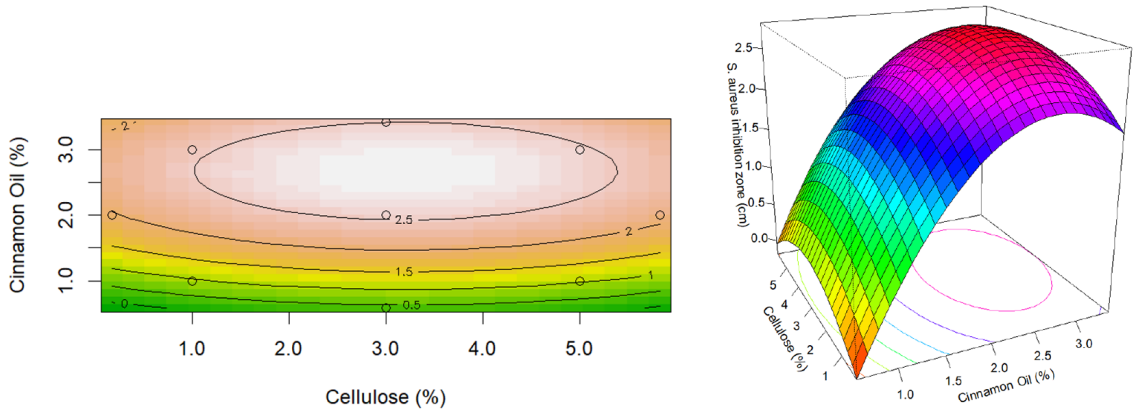

Figure 12. Inhibition zone against *S. aureus*: response surface and contour plot

Inhibition zone assay against *E. coli*

The inhibition zone diameter serves as a direct measure of the antimicrobial effectiveness of the film. The assay was performed against Gram-negative bacteria (*Escherichia coli*) and Gram-positive bacteria (*Staphylococcus aureus*). Figure 11 presents the 3D surface and contour plots illustrating the relationship between cellulose nanofibre (CNF) concentration, cinnamon essential oil (CEO) concentration, and the inhibition zone diameter against *E. coli*.

As it is shown in the response surface, the CEO concentration is the dominant factor driving antimicrobial activity. Increasing the CEO percentage (from 1.0% to 3.0%) results in a distinct, progressive increase in the inhibition zone diameter. This confirms that CEO acts as the primary active agent, where higher loads of cinnamaldehyde allow for greater diffusion of antimicrobial compounds into the agar medium. On the basis of the RSM analysis, the optimum condition for maximising the inhibition zone against *E. coli* was identified at a formulation of 3.0% CEO and 1.0% CNF. Under these conditions, the model predicts a maximum inhibition zone approaching 1.0 cm.

The contour plot further reveals that while CEO is the main driver, the CNF concentration exerts a shielding effect. The highest inhibition values (pink region) are concentrated at lower CNF levels (1.0% – 2.0%) combined with high CEO loads. This suggests that a lower density of nanofibres facilitates a more rapid release and diffusion of the essential oil into the medium, whereas higher CNF concentrations (approaching 5%) may create a denser matrix that slightly restricts the migration of the active compounds.

Response surface methodology analysis of the inhibition zone against *S. aureus*

The interaction between CNF and CEO exerts a more complex and significant effect on *Staphylococcus aureus* compared to *E. coli*. The 3D

surface and 2D contour plots (Figure 12) reveal a distinct convex or dome-shaped" response, indicating a quadratic relationship rather than a simple linear one. Unlike the linear trend observed with *E. coli*, the inhibition zone for *S. aureus* reaches an optimum peak. The contour plot identifies a maximum inhibition zone (exceeding 2.5 cm) in the region of 2.0–2.8% CEO mixed with 2.5–3.5% CNF. This suggests that while increasing CEO initially boosts antimicrobial activity sharply due to higher cinnamaldehyde availability, the effect eventually plateaus or slightly decreases beyond this optimal range. This phenomenon may be due to the saturation of the matrix or a limit to the diffusion rate of the oil at very high concentrations.

Furthermore, the role of CNF is critical in this interaction. The curvature along the CNF axis indicates that a moderate concentration of CNF (approx. 3%) provides the optimal matrix density. If the CNF content is too low, the matrix may be too loose to hold the oil effectively; if too high, the structure may become too compact, hindering the diffusion of the active compounds. Therefore, to maximise the efficacy against Gram-positive *S. aureus*, a specific balance between the structural agent (CNF) and the active agent (CEO) is required. The resulting dark red region on the contour plot highlights these optimal biocomposite formulations, confirming their strong potential for use in active antimicrobial packaging.

CONCLUSIONS

Active food biocomposite films, cassava flour-based matrix that included durian rind CNF as a filler and CEO as an active agent, were successfully produced *via* a solvent and casting process. The optimisation using response surface methodology (RSM) successfully determined that the interaction between CNF and CEO concentrations significantly dictates the performance of the bio-composite film. The optimal formulation was identified at a CNF concentration of 5% and a CEO of 2%, which yielded a maximum tensile strength of 10.45 MPa and a Young's modulus of 188.2 MPa. Regarding water sensitivity, the simultaneous presence of CNF and CEO effectively enhanced the hydrophobicity of the film, reducing the water absorption capacity (WAC) to 37.5%. This is attributed to the hydrophobic nature of the CEO and the ability of CNF to create a denser network within the starch matrix, hindering water molecule penetration. Furthermore, antimicrobial testing confirmed that the inhibition zone expanded significantly with increasing CEO percentages, confirming the efficacy of the film as an active packaging material.

Acknowledgments

The authors thank the Ministry of Education, Culture, Research, and Technology for financial support for this study through the Regular Fundamental Research Grant 2025, with decree number 419/C3/DT.05.00/2025.

REFERENCES

1. Putro J. N. *et al.*, (2022). Cellulose nanocrystals (CNCs) and its modified form from durian rind as dexamethasone carrier, *Polymers*, *14*(23), 5197, https://doi.org/10.3390/polym14235197.
2. Xing H. *et al.*, (2022). Green preparation of durian rind-based cellulose nanofiber and its application in aerogel, *Molecules*, *27*(19), 6507, https://doi.org/10.3390/molecules27196507.
3. Putra Muhammad R. Y.; Yuliati, S., (2024). Pretreatment delignifikasi limbah kulit durian sebagai bahan baku pembuatan bioetanol, *J. Daur Lingkung.*, *7*(2): Agustus, pp. 5–10, 2024, [Online]. http://daurling.unbari.ac.id/index.php/darling/article/view/306/115
4. Suryaningsih W., Budiati T., Muspita Dyah Utami M., Ardhiarisca O., and Candra Dewi A., (2025). Cellulose isolation of durian peel mesocarp as raw material for biofoam manufacture , *J. Ilm. Inov.* *25*(1), SE-Article, 64–71, https://doi.org/10.25047/jii.v25i1.5780.
5. Yong W. S., Yeu Y. L., Chung P. P., andSoon K. H., (2024). Extraction and Characterization of microcrystalline cellulose (MCC) from durian rind for biocomposite application, *J. Polym. Environ.*, *32*(12), 6544–6575, https://doi.org/10.1007/s10924-024-03401-7
6. Pratiwi H., Kusmono, and Wildan M. W., (2023). Oxidized cellulose nanocrystals from durian peel waste by ammonium persulfate oxidation, *ACS Omega*, *8*(33), 30262–30272, https://doi.org/10.1021/acsomega.3c03117
7. Lubis R., Wirjosentono B., Eddiyanto E., and Septevani A., (2020). Preparation and characterization of cellulose pulp from fiber of durian peel, *Rasayan J. Chem.*, *13*, 1767–1776, https://doi.org/10.31788/RJC.2020.1335807
8. Thi Thanh Hop T. *et al.*, (2022). A comprehensive study on preparation of nanocellulose from bleached

wood pulps by TEMPO-mediated oxidation, *Results Chem.*, *4*, 100540, https://doi.org/10.1016/j.rechem.2022.100540

9. Hamidy R., Rachman H., Anggara J., Sulistyo J., and Asri N., (2025). Extraction and characterization of cellulose from Arabica spent coffee grounds, *J. IPTEK*, *29*, 95–104, https://doi.org/10.31284/j.iptek.2025.v29i1.7815
10. Asri N. P. *et al.*, (2025). Environmentally friendly nanofiber cellulose from durian rinds: A sustainable alternative biomass resource, *Asia-Pacific J. Chem. Eng*. e70143, https://doi.org/https://doi.org/10.1002/apj.70143
11. Vyas A., Ng S., Fu T., and Anum I., (2025). ZnO-embedded carboxymethyl cellulose bioplastic film synthesized from sugarcane bagasse for packaging applications, *Polymers*, *17*(5), https://doi.org/10.3390/polym17050579
12. International A., (2018). Standard test method for tensile properties of thin plastic sheeting, *ASTM International Standards*. ASTM International, https://doi.org/10.1520/D0882-18
13. Patterson A. E., Chadha C., Jasiuk I. M., and Allison J. T., (2023). Tensile behavior of individual fibers and films made via material extrusion additive manufacturing, *Next Mater.*, *1*(1), 100002, https://doi.org/10.1016/j.nxmate.2023.100002
14. International A., (2021). Standard test method for haze and luminous transmittance of transparent plastics, *ASTM International Standards*. ASTM International, https://doi.org/10.1520/D1003-21
15. Benitez J. J. *et al.*, (2024). Transparent, plasticized cellulose-glycerol bioplastics for food packaging applications, *Int. J. Biol. Macromol.*, *273*, 132956, https://doi.org/10.1016/j.ijbiomac.2024.132956
16. International A., (2024). Standard test methods for gravimetric determination of water vapor transmission rate of materials, *ASTM International Standards*. ASTM International, https://doi.org/10.1520/E0096_E0096M-24
17. Mohammad Azmin S. N. H., Aliah N., and Mat Nor M. S., (2020). Development and characterization of food packaging bioplastic film from cocoa pod husk cellulose incorporated with sugarcane bagasse fibre, *J. Bioresour. Bioprod.*, *5*, 259–266, https://doi.org/10.1016/j.jobab.2020.10.003
18. Suryanegara L. *et al.*, (2021). Novel antimicrobial bioplastic based on PLA-chitosan by addition of TiO_2 and ZnO, *J. Environ. Heal. Sci. Eng.*, vol. 19, no. 1, pp. 415–425, doi: 10.1007/s40201-021-00614-z.
19. S. R. Masrol, Ibrahim M. H. I. and Adnan S., (2015). Chemi-mechanical pulping of durian rinds, *Procedia Manuf.*, *2*, 171–180, https://doi.org/10.1016/j.promfg.2015.07.030
20. Safira A. and Purbasari A., (2023). Optimization and characterization of biodegradable film based on glutinous flour/glycerol/chitosan/ZnO using Response Surface Methodology (RSM) - Central Composite Design (CCD), *J. Kim. Sains dan Apl.*, *25*, 368–381, https://doi.org/10.14710/jksa.25.10.368-381
21. Rostamabadi H., Bist Y., Kumar Y., Yildirim-Yalcin M., Ceyhan T., and Falsafi S. R., (2024). Cellulose nanofibers, nanocrystals, and bacterial nanocellulose: Fabrication, characterization, and their most recent applications, *Futur. Postharvest Food*, *1*(1), 5–33, https://doi.org/10.1002/fpf2.12001